Probing the Role of Backbone Hydrogen Bonding in β-Amyloid Fibrils with Inhibitor Peptides Containing Ester Bonds at Alternate Positions

David J. Gordon[‡] and Stephen C. Meredith*[,§]

Departments of Biochemistry and Molecular Biology, The University of Chicago, 920 East 58th Street, Chicago, Illinois 60637, and Department of Pathology, The University of Chicago, 5841 Sout Maryland Avenue, Chicago, Illinois 60637

Received April 18, 2002; Revised Manuscript Received October 16, 2002

ABSTRACT: Protein−protein interactions are frequently mediated by stable, intermolecular β-sheets. A number of cytokines and the HIV Protease, for example, dimerize through β-sheet motifs. Evidence also suggests that the macromolecular assemblies of peptides and proteins in amyloid fibrils are stabilized by intermolecular β-sheets. In this paper, we report that interfering with the backbone hydrogen bonding of an amyloidgenic peptide (Aβ16−20) by replacing amide bonds with ester bonds prevents the aggregation of the peptide. The ester bonds were incorporated in an alternating fashion so that the peptide presents two unique hydrogen bonding faces when arrayed in an extended, β-strand conformation; one face of the peptide has normal hydrogen bonding capabilities, but the other face is missing amide protons and its ability to hydrogen bond is severely limited. Analytical ultracentrifugation experiments demonstrate that this ester peptide, Aβ16−20e, is predominantly monomeric under solution conditions, unlike the fibril-forming Aβ16−20 peptide. Aβ16−20e also inhibits the aggregation of the Aβ1−40 peptide and disassembles preformed Aβ1−40 fibrils. These results suggest that backbone hydrogen bonding is critical for the assembly of amyloid fibrils.

Alzheimer's Disease, Huntington's Disease, systemic amyloidoses, and prion diseases, among others, all share the common characteristic of aggregation of peptides and proteins into insoluble amyloid fibrils (*1*, *2*). The aggregating proteins in these diseases include the Aβ[1] peptide in Alzheimer's Disease, huntingtin in Huntington's Disease, the scrapie form of the prion protein (PrP) in the transmissible spongiform encephalopathies, and transthyretin in some forms of familial amyloidoses. Despite a lack of sequence similarity between these soluble proteins, the amyloid fibrils share many common characteristics, including protease resistance and extensive β-sheet structure (*3*, *4*). In addition, amyloid fibrils formed from different proteins exhibit similar fiber diffraction patterns and also interact with the dyes Congo Red and thioflavin T (*3*, *5*, *6*). Despite these similarities, recent solid-state NMR experiments with intact Aβ and various fragments of the Aβ peptide demonstrate that both parallel and antiparallel β-sheet orientations are observed in amyloid fibrils (*7*−*12*). Indeed, it is not surprising that fibrils made from proteins such as transthyretin and immunoglobulin light chains differ in some structural details from fibrils made from short peptides such as β-amyloid.

The common feature of β-sheet structure in amyloid fibrils, formed by proteins that are otherwise structurally diverse, suggests that peptide backbone hydrogen bonding may be important in the assembly and stability of amyloid fibrils. Kheterpal et al. (*13*) recently used hydrogen−deuterium exchange to probe the importance of backbone hydrogen bonding in Aβ1−40 fibrils. These experiments demonstrated that ∼50% of the backbone hydrogen bonds in Aβ1−40 fibrils resist exchange even after 1000 h at room temperature. These data suggest that a highly protected, rigid core structure of backbone hydrogen bonds exists in the amyloid fibril. Although this study did not identify the protected residues, there are two distinctly hydrophobic domains in Aβ1−40: the hydrophobic "core domain" between residues 16−22 and the 12 amino acids at the carboxy terminal of the peptide. It is likely that many of these protected residues are within these two domains.

We, and others, have recently reported that peptides containing *N*-methyl amino acids are effective inhibitors of the fibrillogenesis of Aβ1−40 (*14*−*17*). In our previous work, *N*-methyl groups were placed in alternating positions so that the inhibitor peptides have two unique "faces" when arrayed in a β-strand conformation. One face is capable of forming normal hydrogen bonds with a β-strand partner, but the other face has limited hydrogen bonding capabilities because of the *N*-methyl groups. We observed that several *N*-methyl peptides, based on the hydrophobic core domain of Aβ1−40, both inhibit fibrillogenesis and disassemble preformed fibrils. CD and NMR data indicate that two of these peptides containing *N*-methyl amino acids in alternate

* Corresponding author. E-mail: scmeredi@midway.uchicago.edu.
[‡] Department of Biochemistry and Molecular Biology. Email: djgordon@midway.uchicago.edu
[§] Department of Pathology.

[1] Abbreviations: Aβ, β-amyloid; AD, Alzheimer's Disease; BOC, *tert*-butoxycarbonyl; Bpa, benzoyl-phenylalanine; CD, circular dichroism; DCC, *N*,*N*′-dicyclohexylcarbodiimide; DIC, 1,3-diisopropylcarbodiimide; DMAP, 4-(dimethylamino)-pyridine; DPH, 1,6-diphenyl-1,3,5-hexatriene; FMOC, 9-fluorenylmethoxycarbonyl; HOBt, N-hydroxybenzotriazole; HPLC, high-performance liquid chromatography; HFIP, hexafluoroisopropyl alcohol; IC, inhibitory concentration; MBHA, methylbenzylhydrylamine; TFA, trifluoroacetic acid.

10.1021/bi0259857 CCC: $25.00
Published on Web 12/21/2002

positions, Aβ16−22m and Aβ16−20m, are monomeric β-strands in aqueous solutions (*15*, *16*).

The replacement of amide bonds by ester bonds has been used to investigate the importance of backbone hydrogen bonding since ester bonds lack the amide proton which, in an ordinary peptide, is a potential hydrogen bonding site (*18*−*25*). At the same time, the ester bond shares many structural similarities with the amide bond, such as a predominance of the trans conformation and similar bond lengths and angles (*26*, *27*). In this paper we examine the role of hydrogen bonds in fibrillogenesis through the use of peptides containing ester bonds in the place of amide bonds. We hypothesized that the ester substitutions would yield peptides that were effective inhibitors of fibrillogenesis and would permit a more direct assessment of the role of hydrogen bonds in stabilizing amyloid fibrils than the incorporation of *N*-methyl amino acids. The latter yield peptides with an extraordinarily stable β-strand structure that completely resists denaturation by changes in pH (2−12), temperature (to 70 °C) and the addition of denaturants such as urea or guanidine HCl (to 8M). These results suggest that the *N*-methyl groups confer structural rigidity to the peptides. In addition, a red shift in the CD spectrum of *N*-methyl amino acid-containing peptides suggests that the *N*-methyl groups, while conferring β-strand structure, may also introduce a twist, or distortion, in the β-strand. These findings suggest that *N*-methyl groups may inhibit fibrillogenesis not only by interfering with hydrogen bonding, but also by introducing steric constraints that prevent the close association of β-strands. Such steric constraints could include the relative bulkiness of the *N*-methyl group compared to the amide proton and the twist or distortion of the β-strand caused by the *N*-methyl groups. Both of these factors could interfere with the efficient packing of peptides into fibrillar aggregates. These results, therefore, raise the question of the relative contributions of hydrogen bonding and steric constraints in the ability of these peptides to inhibit Aβ fibrillogenesis.

Thus, the incorporation of ester bonds constitutes a more conservative substitution for peptide bonds than the incorporation of *N*-methyl amino acids. In the studies reported below, we demonstrate that the incorporation of two ester bonds at alternate residues of the Aβ16−20 peptide, similar to the incorporation of *N*-methyl amino acids, prevents the peptide from forming amyloid fibrils. The incorporation of ester bonds also results in the formation of an effective inhibitor of Aβ1−40 fibrillogenesis. Analytical ultracentrifugation demonstrates that the ester peptide is predominantly monomeric, although a small amount of dimeric peptide is observed by cross-linking and ESI-MS experiments, in contrast to *N*-methyl amino acid-containing peptides, which do not form dimers. We will also show that the ester peptide is incorporated into stable, soluble, mixed micelle-like structures with Aβ1−40, i.e., in which the Aβ1−40 does not progress to the formation of fibrils. These results will be interpreted with the goal of understanding the roles of hydrogen bonding and side chain interactions in the formation of β-amyloid fibrils.

MATERIAL AND METHODS

Peptide Synthesis, Purification and Analysis. The Aβ1−40 peptide was synthesized as the C-terminal carboxylic acid using standard 9-fluorenylmethoxycarbonyl and HBTU/HOBt (FastMoc) chemistry on an Applied Biosystems model 431A peptide synthesizer:

$$NH_2-DAEFRHDSGY^{10}\ EVHHQKLVFF^{20}$$
$$AEDVGSNKGA^{30}\ IIGLMVGGVV^{40}-CONH_2$$

Peptides with a carboxamide at the C-terminal were prepared by using an Fmoc−amide MBHA resin (Midwest Biotech). Fmoc−para-benzoyl-phenylalanine (Fmoc−Bpa) was purchased from Bachem. The ester peptides were synthesized using previously described methods (*19*). In short, α-hydroxy acids (2.2 mmol) were coupled to the resin bound peptide using 2.2 mmol of diisopropyl carbodiimide, 2.5 mmol of hydroxybenzotriazole, and 0.8 mmol of *N*-ethylmorpholine in *N*,*N*-dimethylformamide/dichloromethane (1:1, v/v). Coupling was monitored with the Kaiser test and was generally complete within 30 min. The ester bond was formed by activating 2.2 mmol of 9-fluorenylmethoxycarbonyl amino acid with 2.2 mmol of diisopropyl carbodiimide and coupling for 3 h in the presence of 1.2 mmol of *N*-ethylmorpholine and 0.04 mmol of 4-(dimethylamino)pyridine. The peptides were purified using a reverse-phase, C18 preparative HPLC column (Rainin Dynamax) at 60 °C. The solvent system contained 0.1% trifluoroacetic acid in water (solvent A) and 0.1% trifluoroacetic acid in acetonitrile (solvent B). Peptide purity was greater than 97% by analytical HPLC (Rainin C18 column). The molecular masses of the peptides were verified with ESI-MS. For Aβ(16−20)m, m/z = 812.8 (expected = 812.78); for Aβ(16−20)e, m/z = 696.4 (expected = 696.2); for Aβ(16−19)e-Bpa20, m/z = 800.0 (expected = 800.5); and for Prp(117−121)e, m/z = 431.2 (expected = 431.0).

Fibrillogenesis and Fibril Disassembly Assays. The fibril inhibition and disassembly properties of the peptides were measured using a thioflavin T assay described in previous publications (*15*, *28*). For an inhibition assay, the inhibitor peptide, dissolved in HFIP, was divided into aliquots. The HFIP was then evaporated under a stream of dry nitrogen. The dried peptide was resuspended in 100 mM phosphate buffer, 150 mM NaCl, pH 7.4. An aliquot of Aβ1−40 peptide in HFIP was then added to the solution. The mixtures were vortexed for approximately 30 s and then incubated at room temperature for 4 days without shaking. The final concentration of Aβ1−40 in the mixture was 100 μM. The final concentration of HFIP in the assay solutions was less than 2% (v/v), which does not inhibit fibrillogenesis (*29*).

For a disassembly experiment, Aβ1−40 was incubated alone for 4 days to allow fibrils to form, as described in the previous paragraph. An aliquot of the fibrils was then added to inhibitor peptide that had been dried from HFIP. The amount of fibrils remaining intact after a three day incubation at room temperature was assayed using thioflavin T fluorescence and electron microscopy, as described below.

To facilitate the comparison of peptides, the data were fit to the equation for a hyperbola:

$$\%\ \text{Fluorescence} = 100\% - \frac{IC_{max}[P]}{IC_{50} + [P]}$$

where P is the inhibitor:Aβ1−40 ratio and the two param-

eters, IC_{50} and IC_{max}, are analogous to K_m and V_{max}, respectively, of enzyme kinetics. Since a constant concentration of Aβ1−40 was used for these experiments, *P* is a measure of the inhibitor concentration.

Fluorescence Spectroscopy. Fluorescence measurements were performed using a Hitachi F-2000 fluorescence spectrophotometer as described in previous publications (*5*, *15*, *30*). In short, a 5 μL aliquot of solution containing fibrils was injected into 1 mL of a 5 μM thioflavin T solution in 50 mM glycine−NaOH buffer, pH 8.5. The solution was mixed vigorously by vortexing, and the signal was then averaged for 30 s with the excitation and emission wavelengths set to 446 and 490 nm, respectively.

Congo Red Binding. The Congo Red binding assay was performed essentially as described in other publications (*6*). An aliquot of peptide solution containing 50 μg of peptide was added to 1 mL of a 3 μM solution of Congo Red in 100 mM phosphate buffer, pH 7.4. The solution was incubated for 15 min at room temperature and then the absorbance was measured from 400 to 600 nm.

Electron Microscopy. For the electron microscopy, 1−5 μL aliquots (incubation times given above under Fibrillogenesis and Fibril Disassembly Assays) from the inhibition and disassembly samples were applied to a glow-discharge, 400-mesh, carbon-coated support film and stained with 1% uranyl acetate. Micrographs were recorded using a Philips EM300 at magnifications of 17 000, 45 000, and 100 000.

Analytical Ultracentrifugation. Equilibrium analytical ultracentrifugation experiments were performed using a Beckman Optima XLA ultracentrifuge equipped with an An60Ti rotor and analytical cells with six-channel centerpieces. Aβ16−20e was dissolved in 100 mM phosphate buffer, pH 7.4, 150 mM NaCl at concentrations of 0.05, 0.2, and 1 mM. The equilibrium distribution of peptide was measured at 20 °C with rotor speeds of 36 000, 42 000, and 48 000 rpm, corresponding to relative centrifugal fields of 102 000, 139 000, and 181 000 × *g*, respectively, at r_{av} = 7.04 cm. Scans were performed by measuring the UV absorbance at 220 and 256 nm. Twenty scans were averaged at each point with a step size of 0.001 cm. Scans taken 4 h apart were overlaid to determine whether equilibrium had been attained. Partial specific volumes were estimated from amino acid composition and solvent density was calculated using the SEDNTERP program.

Photoaffinity Cross-Linking. Aβ16−19−Bpa20 (500 μM) was incubated either alone or in the presence of a solution of Aβ1−40 (100 μM) for 5 min at room temperature. The mixture was then irradiated at 350 nm in a Hitachi F-2000 fluorescence spectrophotometer for 90 min at room temperature. During the irradiation, aliquots of the mixture were removed at several points and analyzed by SDS−PAGE or MALDI-MS.

SDS−PAGE Analysis. Tris-Tricine SDS−PAGE was performed as described by Schagger and von Jagow (*31*). Coomassie Blue staining was used to detect the peptide bands.

Mass Spectrometry. Matrix-assisted laser desorption ionization-time-of-flight (MALDI-TOF) mass spectrometry was performed using a Perseptive Biosystems Voyager Pro DE (Framingham, MA) instrument in the positive ion mode. The samples were prepared by mixing peptide solutions with an equal volume of α-cyano-4-hydroxycinnamic acid (saturated solution in 50% acetonitrile/0.1% TFA) matrix solution. Approximately 1 μL of the mixture was placed on the sample holder and allowed to dry at room temperature. Spectra of peptides were then acquired in either the linear or reflected mode with an accelerating voltage of 20−25 kV. Each spectrum was produced by accumulating data from 100 to 200 laser shots.

Electrospray ionization mass spectrometry (ESI-MS) was performed using a Perkin-Elmer-Sciex API-300 instrument in the positive ion mode. The peptides were prepared in either deionized water or 5 mM NH_4HCO_3 and infused into the MS at a flow rate of 5 μL/min using a syringe pump. Experiments were performed with a capillary voltage of 5 kV, orifice voltage of 30 V, and a ring voltage of 300 V. Spectra were analyzed using the Biomultiview program provided by the manufacturer (Perkin-Elmer).

DPH Fluorescence. Fluorescence measurements were performed using a Hitachi F-2000 fluorescence spectrophotometer. Samples were prepared as described above for the fibrillogenesis inhibition assay, except that the buffer contained 5 μM 1,6-diphenyl-1,3,5-hexatriene (DPH, Molecular Probes). The fluorescence measurements were taken after incubating the samples for 30 min in the dark. The excitation and emission wavelengths were 358 and 430 nm, respectively.

RESULTS

Peptide Synthesis. Figure 1 shows the peptides synthesized for this work. The unmodified peptide, Aβ16−20 (Figure 1A), is derived from the central, hydrophobic region of Aβ1−40 that is critical for fibrillogenesis. Although this peptide is an inhibitor of Aβ1−40 (*32*), it also aggregates and forms fibrils on its own, as demonstrated below. The ester peptide, Aβ16−20e (Figure 1B), is identical to Aβ16−20 except that it has two ester bonds in alternating positions. When this peptide is arrayed in an extended, β-strand conformation, the oxygen atoms of these ester bonds align on one "face" of the molecule. The *N*-methyl inhibitor peptide described in previous work, Aβ16−20m, is displayed in Figure 1C as a comparison to the ester peptide. This peptide is identical to Aβ16−20e, except that it incorporates *N*-methyl groups, rather than ester groups, in alternating positions. The PrP117−121e peptide (Figure 1D), which also contains two ester bonds, is homologous to a central region of the prion protein and was synthesized to investigate the sequence specificity of the inhibition. The final peptide, Aβ16−19−Bpa20 (Figure 1E), is identical to Aβ16−20e, except that Phe20 is replaced with a photoreactive benzoylphenylalanine (Bpa) amino acid. This peptide is used for cross-linking experiments described below.

The ester peptides were synthesized in excellent purity and yields using established procedures. The stability of the ester bonds to hydrolysis at pH 7.4 was measured using a RP-HPLC assay. Incubation of the ester peptides in 100 mM phosphate buffer, pH 7.4, at 37 °C for 24 h resulted in hydrolysis of 12−14% of the peptide (data not shown). Incubation of the ester peptides at room temperature, however, lowered this rate of hydrolysis to 2% in 24 h (data not shown). All of the experiments reported in this work, consequently, were conducted at room temperature to minimize the hydrolysis of the ester peptides.

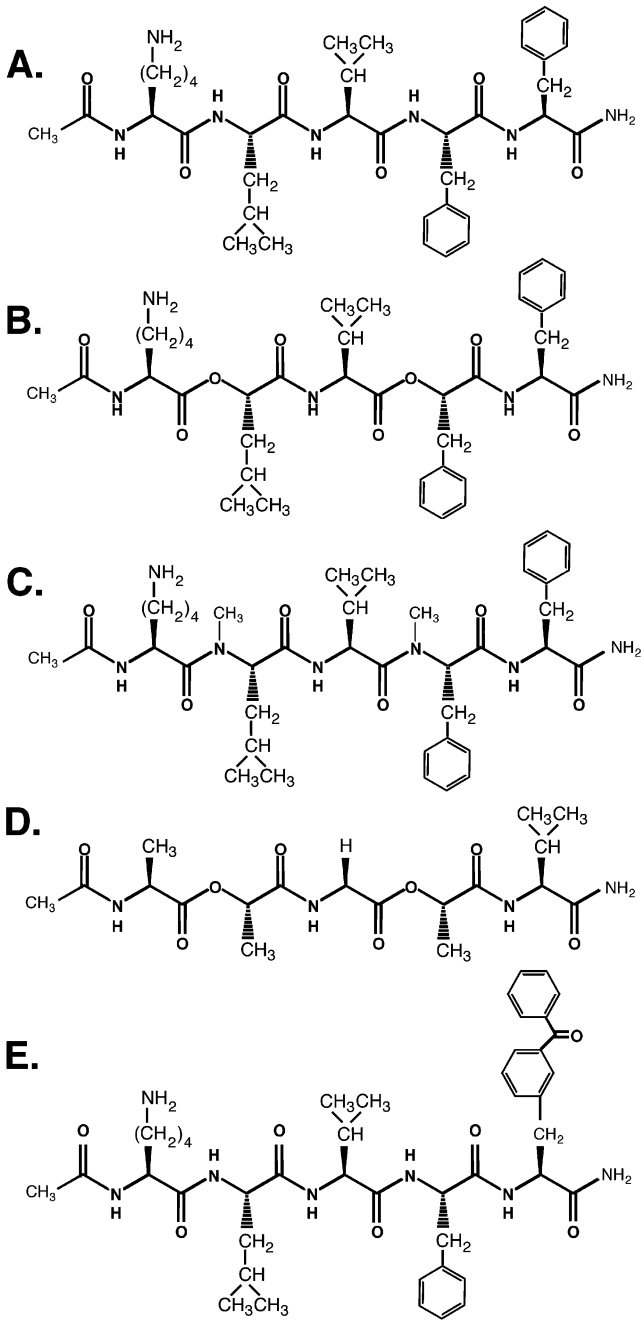

FIGURE 1: Structures of Aβ16−20 (A), Aβ16−20e (B), Aβ16−20m (C), PrP117−121e (D), and Aβ16−19−Bpa20 (E). The figure depicts these structures as single molecules in a β-strand conformation. All of the peptides shown in the figure are based on residues 16−20 of Aβ(1−40), i.e., −KLVFF−; the peptide shown in panel D is based on the sequence of the human prion protein residues 117−121, i.e., −AAGAV−. In the ester and *N*-methyl peptides, the backbone modifications at alternating residues are aligned on one hydrogen bonding face of the β-strand.

Electron Microscopy. Inhibition of Aβ1−40 fibrillogenesis by the ester peptide was initially investigated with electron microscopy. The Aβ1−40 peptide was incubated with different amounts of Aβ16−20e for 4 days at room temperature. Aliquots were then removed from each sample and examined by electron microscopy. The solution of Aβ1−40 incubated in the absence of any inhibitor peptide exhibited long, unbranched fibrils (Figure 2A). Some fibrillar material was also observed when Aβ1−40 was incubated with the Aβ16−20 peptide (Figure 2B). It is not clear, though, if these

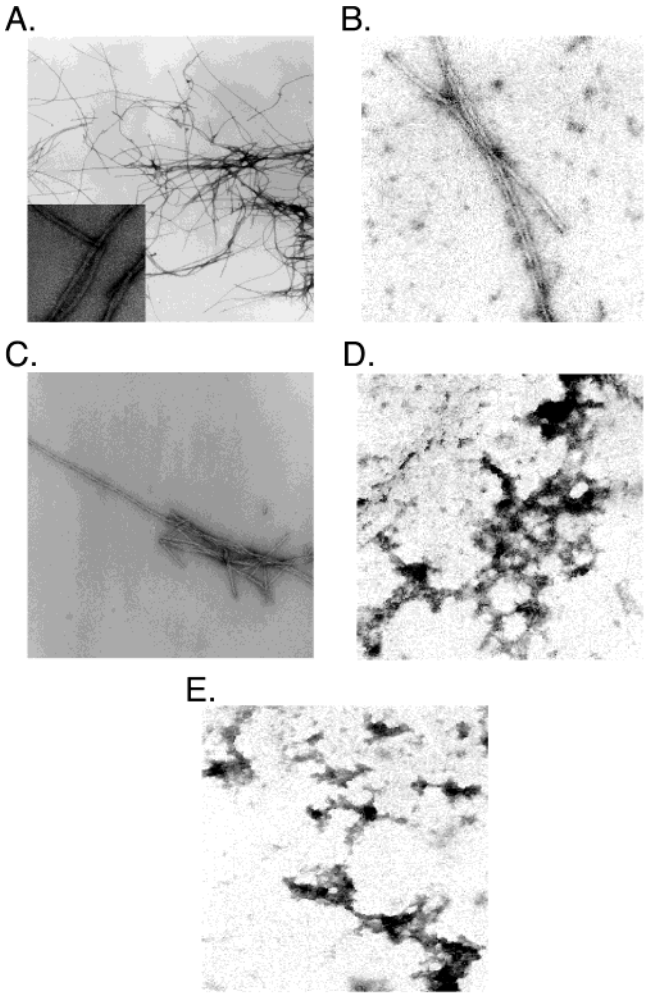

FIGURE 2: Electron micrographs demonstrating the inhibition and disassembly effects of Aβ16−20e and Aβ16−20 on Aβ1−40 fibrillogenesis. (A) Electron micrograph of Aβ1−40 fibrils formed in the absence of any inhibitor peptide. Magnification, ×17 000; inset magnification, ×45 000. (B) Electron micrograph of Aβ1−40 that was incubated with a 20-fold molar excess of Aβ16−20 for 4 days. Magnification, ×45000. (**C**) Electron micrograph of Aβ16−20 incubated in absence of any other peptides. Magnification, ×45000. Panels D and E are electron micrographs of Aβ1−40 incubated with a 20-fold molar excess of Aβ16−20e in an inhibition or disassembly assay, respectively. Magnification, ×45000.

fibrils are composed of Aβ1−40, Aβ16−20 or a mixture of both peptides. As demonstrated in Figure 2C, Aβ16−20 also aggregates to form amyloid fibrils in the absence of any other peptides. Fibrillar material was not observed when Aβ1−40 was incubated with the Aβ16−20e peptide (Figure 2D), although some amorphous material was evident. Similar results were obtained when Aβ16−20e was added to Aβ1−40 fibrils that had been preformed for 4 days before addition of the ester peptide (Figure 2E).

Thioflavin T Assay. A thioflavin T assay was also used as a more quantitative assay for fibrillogenesis. Figure 3A demonstrates that both Aβ16−20 and Aβ16−20e inhibit the fibrillogenesis of Aβ1−40 in a concentration dependent manner. The thioflavin T fluorescence is plotted as a function of the molar ratio of the inhibitor peptide to the Aβ1−40 peptide. Since a constant concentration of Aβ1−40 was used for these experiments, the molar ratio of inhibitor:Aβ1−40 represents the inhibitor concentration. The Aβ16−20e peptide is a more effective inhibitor than Aβ16−20, and its

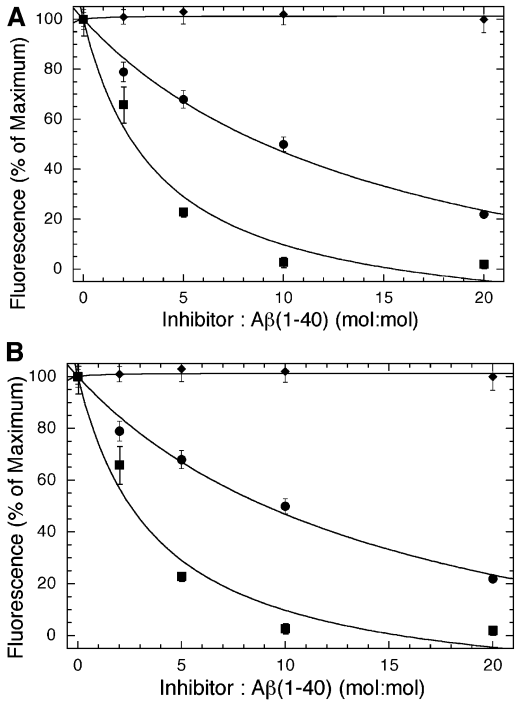

FIGURE 3: Inhibition and disassembly of Aβ1−40 fibrils assayed by thioflavin T fluorescence. In panel A, an inhibition assay, Aβ1−40 was incubated with different amounts of Aβ16−20 (●), Aβ16−20e (■), or PrP117−121e (◆) for 4 days at room temperature. Thioflavin T fluorescence was then measured as described in the Materials and Methods section. Data are expressed as the percentage of signal obtained in the absence of any inhibitor. The curves were fit to an equation for a hyperbola and the parameters derived from least-squares fitting, IC_{50} and IC_{max}, are listed in Table 1. In panel B, a disassembly assay, Aβ1−40 was incubated for 4 days by itself before the inhibitor peptides were added. The samples were then incubated for an additional 3 days, at which time the thioflavin T fluorescence was measured. Symbols are the same as those for panel A.

efficacy is similar to or slightly greater than that of Aβ16−20m. None of the inhibitor peptides cause any thioflavin T fluorescence when incubated alone.

The PrP117−121e peptide does not exhibit any inhibition of Aβ1−40 fibrillogenesis. This demonstrates that the pattern of backbone hydrogen bonds alone is not sufficient to prevent fibrillogenesis, since Aβ16−20e and PrP117−121e exhibit identical backbone hydrogen bonding capabilities. Thus, side chain interactions appear to be critical for the inhibition of fibrillogenesis by Aβ16−20e, as was also observed for the peptides containing *N*-methyl amino acids.

Aβ16−20 and Aβ16−20e are also able to disassemble preformed Aβ1−40 fibrils (Figure 3B). In this experiment, Aβ1−40 was incubated in the absence of any inhibitor for 4 days. At this point, inhibitor peptide was added, and the samples were incubated for an additional 3 days. Similar to the inhibition data, the disassembly of Aβ1−40 fibrils by inhibitor peptides was concentration-dependent, and Aβ16−20e was more effective than Aβ16−20. The PrP117−121e peptide was not able to disassemble Aβ1−40 fibrils, suggesting that disassembly also requires specific side chain interactions.

Studies of Aβ16−20 revealed a subtlety in the use of thioflavin T fluorescence as a technique for measuring the extent of fibril formation by this peptide, or by this peptide in the presence of Aβ1−40. We observed that Aβ16−20 does not induce thioflavin T fluorescence, even under conditions in which Aβ16−20 forms typical amyloid fibrils that are readily visible by electron microscopy. For this reason, thioflavin T fluorescence measurements of Aβ16−20 need to be interpreted cautiously. In the results shown in Figure 3A,B, we observed that the addition of Aβ16−20 to Aβ1−40 leads to a loss of thioflavin fluorescence. It is not possible to say whether this loss of fluorescence results from reduction of fibrillar material, or the presence of fibrils that do not cause thioflavin fluorescence.

Table 1: Summary of Fibril Inhibition and Disassembly Data

	inhibition		disassembly	
peptide	IC_{50}	IC_{max}	IC_{50}	IC_{max}
Aβ16−20e	3.7	100	5.2	100
Aβ16−20m	6.9	100	7.8	100
Aβ16−20	9.7	100	13.5	100
PrP117−121e	nd	nd	nd	nd

The inhibition and disassembly curves were fit to the equation of a hyperbola. The parameters of the hyperbola, IC_{50} and IC_{max}, are analogous to K_m and V_{max} of enzyme kinetics or analogous terms in hyperbolic equations for ligand−receptor interactions. The use of this equation does not imply a specific model for the inhibition by these peptides, such as whether the inhibitor binds Aβ1−40 in the solution or on the fibril. The equation is used to allow a more quantitative comparison of the peptides. The Aβ16−20e peptide exhibits an IC_{50} and IC_{max} for fibril inhibition of 3.7 and 100, respectively (Table 1). These values are similar to or slightly better than the IC_{50} and IC_{max} of Aβ16−20m, 6.9 and 100, reported in a previous publication (*16*). In comparison, the Aβ16−20 peptide exhibits an IC_{50} of 9.7 and an IC_{max} of 100. Although it is difficult to compare different amyloid inhibitors directly, the Aβ16−20e peptide is approximately as effective as other peptide inhibitors of amyloid fibrillogenesis (*40*, *41*).

Congo Red Assay. Thioflavin T fluorescence is well-known as a sensitive assay for the formation of amyloid fibrils. As shown above and by others (*42*, *50*, *51*), however, some peptides that form typical amyloid fibrils do not cause thioflavin fluorescence, either because the fibrils do not bind thioflavin or because binding of the dye by some proteins or peptides is not associated with fluorescence. Neither Aβ16−22 nor Aβ16−20 fibrils, for example, bind thioflavin, despite the fact that both peptides form typical amyloid fibrils visible by electron microscopy and bind Congo Red dye. For this reason, a Congo Red binding assay was also used to investigate both the formation of amyloid fibrils and the inhibition and disassembly of Aβ1−40 fibrillogenesis (Figure 4). Congo Red, an azo dye, exhibits a characteristic increase and redshift in its absorbance spectrum when it binds to amyloid fibrils. Figure 4A demonstrates that both fibrillar Aβ1−40 and Aβ16−20 bind Congo Red, in agreement with the results from electron microscopy. The Aβ16−20e peptide alone, however, does not cause a change in the absorbance spectrum of Congo Red, suggesting that it does not aggregate to form amyloid fibrils, again in agreement with results from electron microscopy.

Figure 4B shows the results of a Congo Red binding assay for Aβ1−40 incubated with Aβ16−20e and for preformed Aβ1−40 fibrils to which Aβ16−20e was added. In both

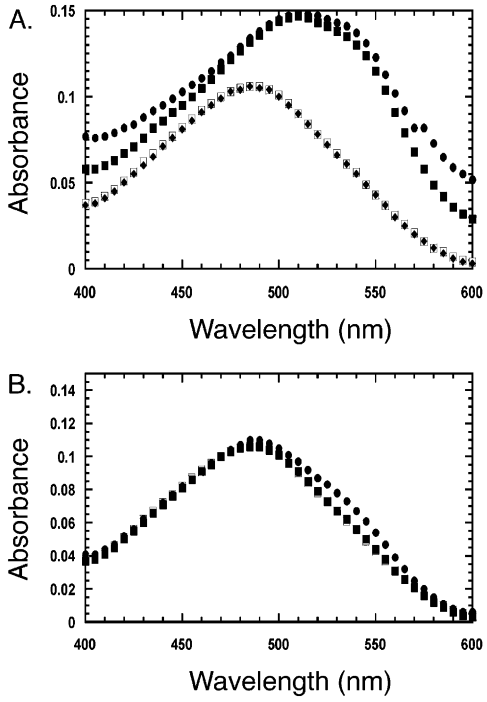

FIGURE 4: Inhibition and disassembly of Aβ1−40 fibrils assayed by Congo Red. In panel A, approximately 50 μg of Aβ1−40 (●), Aβ16−20 (■), or Aβ16−20e (◆) that had been incubated for 4 days at room temperature was added to 1 mL of a 3 μM Congo Red solution. After a 15 min incubation, the absorbance was measured from 400 to 600 nm. The absorbance of the Congo Red solution (□) in the absence of any added peptides is also shown for comparison. In panel B, Aβ16−20e was incubated with Aβ1−40 in an inhibition (●) or disassembly (■) assay. Samples were measured as described for panel A. The absorbance spectrum of Congo Red (□) in the absence of any peptides is again shown for comparison.

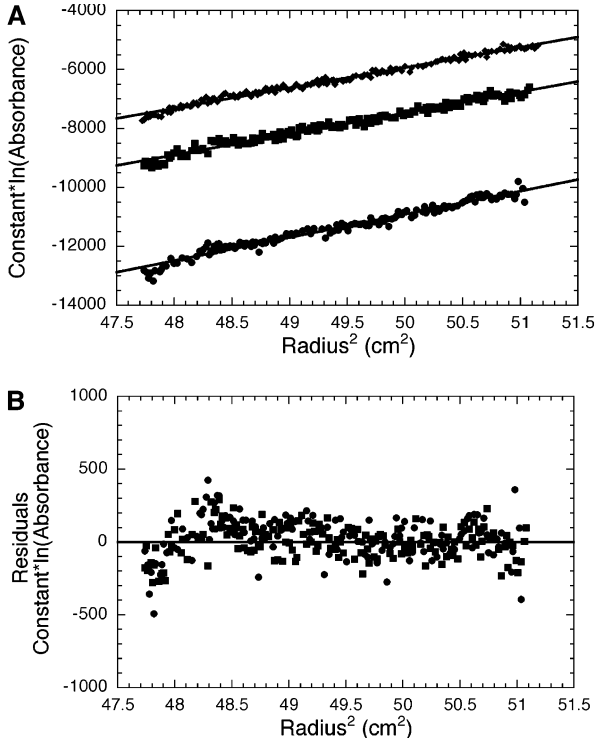

FIGURE 5: (A) Equilibrium analytical ultracentrifugation of a 1 mM solution of Aβ16−20e in buffer (100 mM phosphate, 150 mM NaCl, pH 7.4) at 36 000 (●), 42 000 (■), and 48 000 (◆) rpm. The data are displayed as normalized log plots. The solid lines drawn through the data were obtained by fitting the ln(absorbance) vs radius^2 data to an equation of a single ideal species. Higher order fits resulted in poorer agreement with the experimental data. The residual differences between the experimental data and theoretical curves are plotted in panel B.

cases, the spectra for these mixtures are identical to the control spectrum of Congo Red alone. These results demonstrate that Aβ16−20e does not form fibrils by itself and both inhibits fibril formation and disassembles preformed Aβ1−40 fibrils.

Analytical Ultracentrifugation. Analytical ultracentrifugation was used to determine if the Aβ16−20e peptide forms small aggregates or oligomers. Data were collected at three rotor speeds on solutions containing three different concentrations of Aβ16−20e, 0.05, 0.2, and 1 mM. Data are shown in Figure 5 for the most concentrated, 1 mM, solution of Aβ16−20e. The calculated molecular weight of Aβ16−20e is 695.87 Da. A molecular weight of 734 ± 32 Da was measured in the ultracentrifugation experiment for Aβ16−20e, indicating that the peptide is predominantly or entirely monomeric.

Mass Spectrometry. The aggregation of Aβ16−20e was also investigated using ESI-MS, which is an established technique for studying noncovalent protein complexes (*43*−*46*). Figure 6A is an ESI mass spectrum for a 250 μM solution of Aβ16−20e. This spectrum exhibits two major peaks at *m*/*z* 696.4 and 1392.4 Da (all *m*/*z* values ± 1 Da). Since the calculated molecular weight of monomeric Aβ16−20e is 695.87 Da, the peak at 1392.4 Da demonstrates that the peptide forms a dimeric species under the conditions of ESI-MS. The ESI mass spectrometry spectrum for Aβ16−20 also exhibits a major peak at the molecular weight for a dimeric peptide (Figure 6B). In comparison, the spectrum for the Aβ16−20m peptide exhibits at most only a very minor peak at the molecular weight for a dimeric species (Figure 6C).

Bpa Cross-Linking. The mass spectrometry data demonstrate that Aβ16−20e forms a dimer in solution. Since peak intensities in ESI depend on many factors and are generally not considered quantitative, we were unable to estimate the fractions of monomeric and dimeric Aβ16−20e. The analytical ultracentrifugation results, however, suggest that Aβ16−20e is predominantly monomeric (>90%) because the measured molecular weight is close to the monomer weight and the data are best fit by a single ideal species model, as opposed to a monomer−dimer model.

To examine the ESI-MS data further, we synthesized an analogue of Aβ16−20e, Aβ16−19e-Bpa20, that contains a photoreactive L-*p*-benzoylphenylalanine (Bpa) amino acid (Figure 1E). After activation at 350−360 nm, Bpa preferentially reacts with unreactive C−H bonds, even in the presence of water and other nucleophiles (Figure 7A). Photoaffinity labeling with Bpa is highly efficient and generally exhibits excellent site specificity, somewhat favoring C−H bonds adjacent to heteroatoms (*47*−*49*). Figure 7B shows the MALDI mass spectrometry results for a 500 μM solution of Aβ16−19−Bpa20 that was irradiated at 350 nm for 30 min. Although most of the Aβ16−20e is monomeric (MW= 800.1 Da), after the irradiation a dimer (MW= 1624.1 Da) peak is also observed in the mass spectrum, which is consistent with both the ESI-MS and AUC data. In contrast to ESI-MS, a noncovalent dimer of

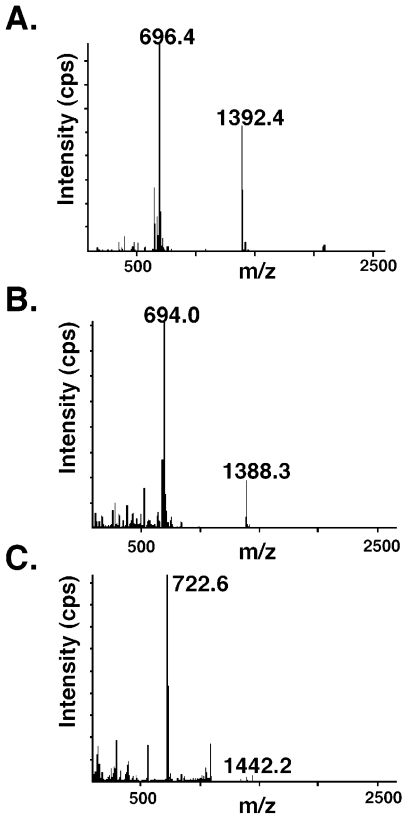

FIGURE 6: ESI-MS detects noncovalent dimers of the Aβ peptides. Shown are ESI-MS spectra of 250 μM solutions of Aβ16−20e (A), Aβ16−20 (B), and Aβ16−20m (C). The samples were prepared in deionized water, and the data were collected as described in the Materials and Methods section. The peaks corresponding to the monomer and dimer molecular weights for each peptide are labeled on the spectra.

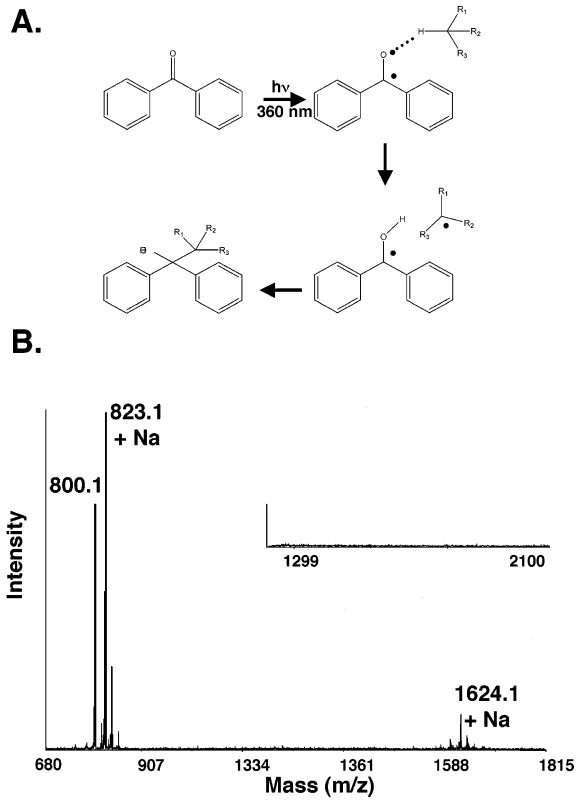

FIGURE 7: Aβ16−19−Bpa20 forms a covalent dimer upon irradiation with UV light. The MALDI-MS spectrum of a 500 μM solution of Aβ16−19−Bpa20 irradiated for 30 min at 350 nm shows peaks at 800.1 and 1624.1 Da, corresponding to monomeric and dimeric Aβ16−20−Bpa, respectively. The inset panel demonstrates that in the absence of irradiation, the dimer peak at 1624.1 Da is not observed in the MALDI-MS spectrum.

Aβ16−19−Bpa20 is not observed by MALDI-MS; the inset of Figure 7B demonstrates that cross-linking does not occur in absence of irradiation.

Aβ1−40 and Bpa Cross-Linking. The Aβ16−19−Bpa20 peptide was also reacted with Aβ1−40 to determine the binding stoichiometry. Figure 8A shows SDS−PAGE results of Aβ16−19−Bpa20 incubated with Aβ1−40 for various amounts of time. Irradiation of the mixture results in the formation of a complex with a molecular weight slightly greater than Aβ1−40 alone. Figure 8B shows MALDI-MS analysis of the irradiated Aβ1−40 and Aβ16−19−Bpa20 mixture. Unmodified Aβ1−40 is represented by the peak at 4330.4. The peaks at 5132.6 and 5931.5 Da correspond to Aβ1−40 cross-linked to one and two Aβ16−19−Bpa20 peptides, respectively. This experiment, however, cannot address the question of whether the Aβ1−40, to which Aβ16−19−Bpa20 is bound, is in a monomeric or oligomeric form because Aβ1−40 is only cross-linked to Aβ16−19−Bpa20 and not to itself.

DPH Fluorescence. To investigate the state of aggregation of the Aβ1−40 peptide that was cross-linked to Aβ16−20e, we used a 1,6-diphenyl-1,3,5-hexatriene (DPH) fluorescence assay. DPH is a hydrophobic dye that exhibits a characteristic increase in fluorescence when it partitions into a hydrophobic environment. This dye was previously used to monitor the formation of a micelle-like Aβ1−40 oligomer that forms within thirty minutes of the peptide being dissolved in solution (*53*). Figure 9A confirms data originally generated by Soreghan et al. (*53*) and shows the effect of increasing Aβ1−40 concentrations on the fluorescence of DPH. Very little DPH fluorescence is observed below the critical concentration of approximately 100 μM Aβ1−40. Above this concentration, though, there is a significant increase in DPH fluorescence with increasing peptide concentration. Figure 9B demonstrates that Aβ16−20e, even when added at a large molar excess relative to Aβ1−40, does not inhibit the formation of the micelle-like intermediate of Aβ1−40. DPH fluorescence is plotted as a function of the molar ratio of the inhibitor peptide to the Aβ1−40 peptide. In all samples, the concentration of Aβ1−40 is 150 μM, and only the concentration of Aβ16−20e is varied. DPH fluorescence is not observed for either the Aβ16−20e peptide alone or monomeric Aβ1−40 in a 9M urea solution (data not shown).

DISCUSSION

The replacement of an amide bond with an ester bond is an established method for investigating the role of backbone hydrogen bonding. The ester group is a conservative substitution for the amide group because both the ester and amide bond adopt predominantly a trans, planar conformation and share similar Ramachandran plots (*26*, *27*). The primary difference between the amide and ester bond is that the hydrogen bond donating amide NH is replaced with an electronegative oxygen atom. In addition, the ester carbonyl is less basic than the amide carbonyl and, as a consequence, is a weaker hydrogen bond acceptor (*54*).

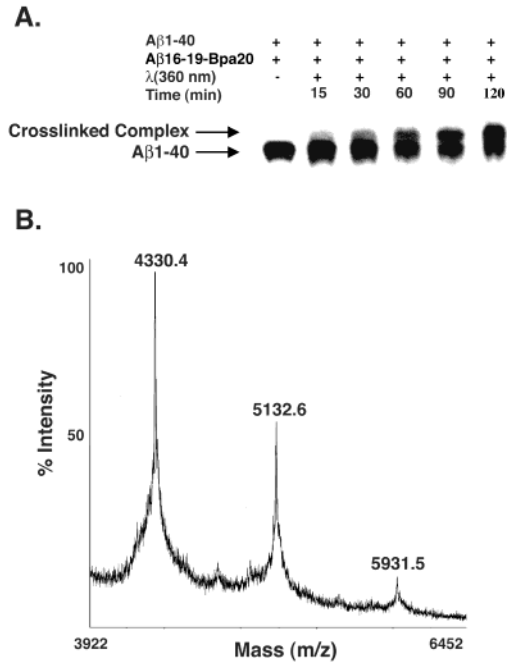

FIGURE 8: Aβ16−19−Bpa20 is cross-linked to Aβ1−40 upon irradiation with UV light for 90 min at room temperature. Panel A shows SDS−PAGE gel analysis of a mixture of Aβ16−19−Bpa20 and Aβ1−40 that was incubated in the absence (lane 1) or presence (lanes 2, 3, 4, 5, and 6) of near-UV light for different amounts of time. Panel B shows MALDI-MS analysis of the Aβ16−19−Bpa20 and Aβ1−40 mixture after exposure to near-UV light. The peak at 4330.4 Da represents the monomeric Aβ1−40 peptide. The peaks at 5132.6 and 5931.5 Da correspond to Aβ1−40 cross-linked to one and two Aβ16−19−Bpa20 peptides, respectively.

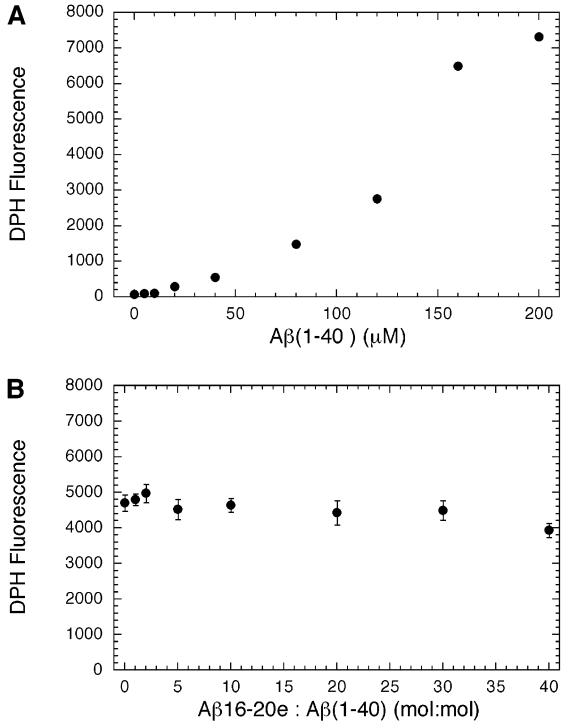

FIGURE 9: DPH fluorescence in the presence of Aβ1−40 and a mixture of Aβ1−40 and Aβ16−20e. Panel A shows the effect of Aβ1−40 concentration on DPH fluorescence. Lyophilized Aβ1−40 peptide was dissolved in 100 mM phosphate buffer, 150 mM NaCl, pH 7.4 containing 5 μM diphenylhexatriene. Samples were incubated in the dark for 30 min prior to measuring the fluorescence. In panel B, Aβ1−40 was incubated with different amounts of Aβ16−20e for 30 min in the dark in buffer containing 5 μM diphenylhexatriene. Data are expressed as the percentage of signal obtained in the absence of any Aβ16−20e peptide.

This strategy of replacing amide bonds with ester bonds has been employed in a number of studies investigating both intramolecular and intermolecular hydrogen bonding interactions (*18*−*25*). Lu et al., for example, used an amide-to-ester replacement to investigate an intermolecular hydrogen bond stabilizing a protease-inhibitor complex (*20*, *21*). Similarly, Schultz et al. utilized ester bonds to probe hydrogen bonding in both α-helix and β-sheet secondary structures (*23*, *24*). Recently, Beligere et al. replaced four amide bonds that span the length of a helix in chymotrypsin inhibitor 2 with ester bonds and demonstrated that the protein folds into a functional, although destabilized, structure (*25*).

Thus, we compared the Aβ16−20e peptide to both the unmodified congener Aβ16−20 and the inhibitor peptide Aβ16−20m for its ability to form fibrils and inhibit the fibrillogenesis of Aβ1−40 and disassemble preformed Aβ1−40 fibrils. All three peptides inhibit fibrillogenesis and disassemble preformed fibrils; the efficacy of Aβ16−20e is similar to that of Aβ16−20m, both of which are better inhibitors than Aβ16−20. Aβ16−20, though an inhibitor of fibrillogenesis, resembles its parent peptide, Aβ1−40, in that it forms fibrils by itself. The Aβ16−20 fibrils appear by electron microscopy as long, unbranched amyloid fibrils and cause the typical redshift in the spectrum of Congo Red dye. These fibrils do not induce thioflavin T fluorescence, however, a trait shared by other short amyloidogenic peptides (*42*, *50*, *51*). In contrast to Aβ16−20, neither Aβ16−20m nor Aβ16−20e forms fibrils, as shown by electron microscopy, and by thioflavin T and Congo Red binding assays.

A molecular weight of approximately 730 Da was obtained for Aβ16−20e by analytical ultracentrifugation, which demonstrates that this peptide is predominantly monomeric in solution. A disadvantage of analytical ultracentrifugation, however, is that it is often difficult to identify weakly aggregating species, particularly for low molecular weight peptides (*52*). A small amount of a dimeric peptide in the presence of predominantly monomeric peptide, for example, is not readily identifiable by analytical ultracentrifugation.

In recent years, ESI-MS has emerged as a powerful technique for studying weak, noncovalent interactions between proteins or between proteins and other ligands (*43*−*46*). Unlike other techniques, such as analytical ultracentrifugation and size exclusion chromatography, ESI mass spectrometry provides the exact molecular weight of a complex, even in the presence of high concentrations of other species. In electrospray ionization, charged droplets are generated at atmospheric pressure by spraying a sample under a strong electric field. This ionization process is very "soft" and leaves the ions largely unfragmented, which facilitates the observation of noncovalent complexes. Chen et al. (*56*), for example, used ESI-MS to investigate the conformation and aggregation of the Aβ1−40 peptide. In these experiments, monomeric, dimeric, trimeric, and tetrameric Aβ1−40 species were observed by ESI-MS.

ESI-MS analysis of Aβ16−20 and Aβ16−20e demonstrate that both of these peptides form dimers in solution. The cross-linking results for the Aβ16−19−Bpa20 peptide are consistent with both the AUC and ESI-MS data because they demonstrate that Aβ16−20e forms a small amount of a dimeric species in solution, which is not readily detectable

by analytical ultracentrifugation. ESI-MS concentrates and desolvates peptides, and for this reason, the results of ESI-MS are difficult to compare directly and quantitatively with those of analytical ultracentrifugation. The *N*-methyl peptide does not appear to form a dimer to nearly the same extent as Aβ16−20 or Aβ16−20e. This is consistent with the recent report of a pentapeptide, unrelated to Aβ, that contains two alternating *N*-methyl amino acids and exhibits a $K_d > 150$ mM for dimerization (*57*).

These observations are also consistent with our previous proposal that Aβ16−20m and other *N*-methylated peptides form distorted or twisted β-strands, which severely hinders the formation of dimers. Aβ16−20e, in contrast, can form a dimer, albeit at high concentrations. The high concentration of Aβ16−20e needed for dimerization indicates a very low affinity constant for dimerization. Nevertheless, these results suggest that the ester represents a more conservative substitution than the *N*-methyl amino acid and more fully preserves the geometry of the unmodified peptide bond. We infer, therefore, that the inability of Aβ16−20e to form fibrils, in contrast to the ability of Aβ16−20 to do so, is attributable mainly or completely to the loss of two hydrogen bonding sites resulting from the use of ester bonds in place of amide bonds in the peptide backbone.

The similar inhibitory properties of Aβ16−20e compared to Aβ16−20m also suggest that interfering with hydrogen bonding is sufficient to prevent Aβ1−40 fibrillogenesis and that steric contributions from the *N*-methyl group are not required. Cross-linking experiments demonstrate that primarily one Aβ16−19−Bpa20 binds to each Aβ1−40 peptide. On the basis of the DPH fluorescence experiments and the electron microscopy, it is likely that the Aβ16−20e peptide is interacting with an oligomeric, rather than monomeric, form of Aβ1−40.

The detailed pathway of Aβ1−40 aggregation is incompletely described. Current data support a nucleation-polymerization model which proposes that below a critical concentration of Aβ1−40 the peptide is monomeric and does not aggregate (*58*). If the critical concentration is exceeded, then small nuclei form during a slow, lag phase. These nuclei then "seed" the rapid self-assembly of additional Aβ1−40 during the polymerization phase. A number of intermediates, variously termed oligomers, prefibrils, and protofibrils, have been postulated to exist at points during fibrillogenesis. None of these intermediates have been isolated or characterized, however. The temporal relationship of these intermediates is also unclear.

Glabe and associates have shown that Aβ1−40 forms a micelle-like structure that binds DPH. Neutron and light scattering experiments have identified a micelle-like Aβ1−40 oligomer that is composed of approximately 30−50 peptides and forms early on the fibrillogenesis pathway (*59*−*61*). Temporal analysis of the fibril length distribution suggests that this micelle structure may be the center of fibril nucleation (*60*). It is not clear, though, if this is the same oligomer that interacts with DPH. Cross-linking Aβ1−40 with a variety of reagents typically reveals a banding pattern with a monomer−hexamer stoichiometry (*29*, *62*). It is not clear if the scattering and cross-linking experiments are both monitoring the same intermediate. Similarly, it is not known which intermediates interact with DPH.

The data in this paper demonstrate that Aβ16−20e blocks the polymerization of Aβ1−40 before the formation of the species that binds thioflavin T. We confirmed the findings of Glabe and associates that Aβ1−40 forms a DPH-binding, micelle-like structure with a "critical micelle concentration" of $\sim$100 μM. Our data also suggest that Aβ16−20e functions by associating with the intermediate that binds DPH. Addition of Aβ16−20e to a molar excess of 40:1 compared to Aβ1−40 had little effect on DPH fluorescence, suggesting that the addition of Aβ16−20e was compatible with preservation of a micelle-like structure. Furthermore, at the concentrations of Aβ16−20e and Aβ1−40 used in this experiment, Aβ16−20e forms a cross-linkable, equimolar complex with Aβ1−40. Since the complex of Aβ16−20e and Aβ1−40 is stable in solution, our data suggest that the Aβ16−20e peptide stabilizes a micelle-like—i.e., DPH binding—form of Aβ1−40, in such a way that the complex does not progress toward the formation of fibrils. It is not known if this micelle structure is an on- or off-pathway intermediate of fibrillogenesis. Consequently, it is possible that the inhibitor peptide either traps an off-pathway intermediate or blocks the progression to fibrils from an on-pathway intermediate. The data in this paper, however, do not exclude the possibility that the inhibitor peptides also bind to the fibril surface, or another form of the Aβ1−40 peptide.

In this paper, we have shown that incorporation of ester bonds into the Aβ16−20 peptide prevents it from aggregating and forming amyloid fibrils. By placing the ester bonds in alternating positions, Aβ16−20e was designed to display, in a β-strand conformation, one normal hydrogen bonding face and one face with diminished hydrogen bonding capabilities due to the absence of amide protons. While this modification prevented the peptide from forming amyloid fibrils, mass spectrometry and cross-linking demonstrated that Aβ16−20e is still able to form a dimeric species in solution. This feature contrasts with Aβ16−20m, in which the *N*-methyl groups appear to disfavor self-association strongly, even at the level of a dimer. The Aβ16−20e peptide also inhibits the fibrillogenesis of Aβ1−40 and disassembles preformed Aβ1−40 fibrils. It remains an open question, though, whether disruption of β-amyloid fibrils is therapeutically advantageous or disadvantageous. Indeed, strong arguments for either side can be found in the literature. Nevertheless, our data suggest that interfering with the backbone hydrogen bonding of amyloidgenic proteins is a feasible goal, should this prove to be therapeutically warranted.

ACKNOWLEDGMENT

We thank the Alzheimer's Association (IIRG 98-1344 and the NIH (5 T32 GM07281, D.J.G.) for support of this work.

REFERENCES

1. Koo, E. H., Lansbury, P. T., Jr, and Kelly, J. W. (1999) Amyloid diseases: abnormal protein aggregation in neurodegeneration, *Proc. Natl. Acad. Sci. U.S.A. 96*, 9989−9990.
2. Kelly, J. W. (2000) Mechanisms of amyloidogenesis, *Nat. Struct. Biol. 7*, 824−826.
3. Sipe, J. D. (1992) Amyloidosis, *Annu. Rev. Biochem. 61*, 947−975.
4. Inouye, H., Fraser, P. E., and Kirschner, D. A. (1993) Structure of β-crystallite assemblies formed by Alzheimer β-amyloid protein analogues: analysis by X-ray diffraction, *Biophys. J. 64*, 502−519.

5. Naiki, H., and Nakakuki, K. (1996) First-order kinetic model of Alzheimer's β-amyloid fibril extension in vitro, *Lab. Invest. 74*, 374−383.
6. Klunk, W. E., Pettegrew, J. W., and Abraham, D. J. (1989) Quantitative evaluation of Congo Red binding to amyloid-like proteins with a β-pleated sheet conformation, *J. Histochem. Cytochem. 37*, 1273−1281.
7. Benzinger, T. L., Gregory, D. M., Burkoth, T. S., Miller-Auer, H., Lynn, D. G., Botto, R. E., and Meredith, S. C. (2000) Two-dimensional structure of β-amyloid(10−35) fibrils, *Biochemistry 39*, 3491−3499.
8. Benzinger, T. L., Gregory, D. M., Burkoth, T. S., Miller-Auer, H., Lynn, D. G., Botto, R. E., and Meredith, S. C. (1998) Propagating structure of Alzheimer's beta-amyloid(10−35) is parallel β-sheet with residues in exact register, *Proc. Natl. Acad. Sci. U.S.A. 95*, 13407−13412.
9. Gregory, D. M., Benzinger, T. L., Burkoth, T. S., Miller-Auer, H., Lynn, D. G., Meredith, S. C., and Botto, R. E. (1998) Dipolar recoupling NMR of biomolecular self-assemblies: determining inter- and intrastrand distances in fibrilized Alzheimer's β-amyloid peptide, *Solid State Nucl. Magn. Reson. 13*, 149−166.
10. Antzutkin, O. N., Balbach, J. J., Leapman, R. D., Rizzo, N. W., Reed, J., and Tycko, R. (2000) Multiple quantum solid-state NMR indicates a parallel, not antiparallel, organization of β-sheets in Alzheimer's β-amyloid fibrils, *Proc. Natl. Acad. Sci. U.S.A. 97*, 13045−13050.
11. Balbach, J. J., Ishii, Y., Antzutkin, O. N., Leapman, R. D., Rizzo, N. W., Dyda, F., Reed, J., and Tycko, R. (2000) Amyloid fibril formation by Aβ16−22, a seven-residue fragment of the Alzheimer's β-amyloid peptide, and structural characterization by solid state NMR, *Biochemistry 39*, 13748−13759.
12. Lansbury, P. T., Costa, P. R., Griffiths, J. M., Simon, E. J., Auger, M., Halverson, K. J., Kocisko, D. A., Hendsch, Z. S., Ashburn, T. T., and Spencer, R. G. (1995) Structural model for the β-amyloid fibril based on interstrand alignment of an antiparallel-sheet comprising a C-terminal peptide, *Nat. Struct. Biol. 2*, 990−998.
13. Kheterpal, I., Zhou, S., Cook, K. D., and Wetzel, R. (2000) Aβ amyloid fibrils possess a core structure highly resistant to hydrogen exchange, *Proc. Natl. Acad. Sci. U.S.A. 97*, 13597−13601.
14. Hughes, E., Burke, R. M., and Doig, A. J. (2000) Inhibition of toxicity in the β-amyloid peptide fragment beta-(25−35) using N-methylated derivatives: a general strategy to prevent amyloid formation, *J. Biol. Chem. 275*, 25109−25115.
15. Gordon, D. J., Sciarretta, K. L., and Meredith, S. C. (2001) Inhibition of β-amyloid(40) fibrillogenesis and disassembly of β-amyloid(40) fibrils by short β-amyloid congeners containing N-methyl amino acids at alternate residues, *Biochemistry 40*, 8237−8245.
16. Gordon, D. J., Tappe, R., and Meredith, S. C.(2002) Design and characterization of a membrane permeable N-methyl amino acid-containing peptide that inhibits Aβ1−40 fibrillogenesis, *J. Pept. Res. 60*, 37−55.
17. Kapurniotu, A., Schmauder, A., and Tenidis, K. (2002) Structure-based design and study of non-amyloidogenic, double N-methylated IAPP amyloid core sequences as inhibitors of IAPP amyloid formation and cytotoxicity, *J. Mol. Biol. 315*, 339−350.
18. Bramson, H. N., Thomas, N. E., and Kaiser, E. T. (1985) The use of *N*-methylated peptides and depsipeptides to probe the binding of heptapeptide substrates to cAMP-dependent protein kinase, *J. Biol. Chem. 260*, 15452−15457.
19. Coombs, G. S., Rao, M. S., Olson, A. J., Dawson, P. E., and Madison, E. L. (1999) Revisiting catalysis by chymotrypsin family serine proteases using peptide substrates and inhibitors with unnatural main chains, *J. Biol. Chem. 274*, 24074−24079.
20. Lu, W., Randal, M., Kossiakoff, A., and Kent, S. B. (1999) Probing intermolecular backbone H-bonding in serine proteinase-protein inhibitor complexes, *Chem. Biol. 6*, 419−427.
21. Lu, W. Y., Starovasnik, M. A., Dwyer, J. J., Kossiakoff, A. A., Kent, S. B., and Lu, W. (2000) Deciphering the role of the electrostatic interactions involving Gly70 in eglin C by total chemical protein synthesis, *Biochemistry 39*, 3575−3584.
22. Arad, O., and Goodman, M. (1990) Depsipeptide analogues of elastin repeating sequences: synthesis, *Biopolymers. 29*, 1633−1649.
23. Chapman, E., Thorson, J. S., and Schultz, P. G. (1997) Mutational analysis of backbone hydrogen bonds in staphylococcal nuclease, *J. Am. Chem. Soc. 119*, 7151−7152.
24. Koh, J. T., Cornish, V. W., and Schultz, P. G. (1997) An experimental approach to evaluating the role of backbone interactions in proteins using unnatural amino acid mutagenesis, *Biochemistry 36*, 11314−11322.
25. Beligere, G. S., and Dawson, P. E. Design, synthesis and characterization of 4-ester CI2, a model for backbone hydrogen bonding in protein α-helices, *J. Am. Chem. Soc. 122*, 12079−12082 (2000).
26. Wiberg, K. B., and Laidig, K. E. (1987) Barries to rotation adjacent to double bonds. 3. The C−O barrier in formic acid, methyl formate, acetic acid, and methyl acetate. The origin of ester and amide resonance, *J. Am. Chem. Soc. 109*, 5935−5943.
27. Ingwall, R. T., and Goodman, M. (1974) Polydepsipeptides. III. Theoretical conformational analysis of randomly coiling and ordered depsipeptide chains, *Macromolecules 7*, 598−605.
28. Jarrett, J. T., Berger, E. P., and Lansbury, P. T. (1993) The carboxy terminus of the β-amyloid protein is critical for the seeding of amyloid formation- Implications for the pathogenesis of Alzheimer's Disease, *Biochemistry 32*, 4693−4697.
29. Levine, H. 3rd. (1995) Soluble multimeric Alzheimer β(1−40) pre-amyloid complexes in dilute solution. *Neurobiol. Aging. 16*, 755−764.
30. Naiki, H., Higuchi, K., Hosokawa, M., and Takeda, T. (1989) Fluorometric determination of amyloid fibrils in vitro using the fluorescent dye, thioflavin T1, *Anal. Biochem. 177*, 244−249.
31. Schagger, H., and von Jagow, G. (1987) Tricine-sodium dodecyl sulfate-polyacrylamide gel electrophoresis for the separation of proteins in the range from 1 to 100 kDa, *Anal. Biochem. 166*, 368−379.
32. Tjernberg, L. O., Naslund, J., Lindqvist, F., Johansson, J., Karlstrom, A. R., Thyberg, J., Terenius, L., and Nordstedt, C. (1996) Arrest of beta-amyloid fibril formation by a pentapeptide ligand, *J. Biol. Chem. 271*, 8545−8548.
33. Hilbich, C., Kisters-Woike, B., Reed, J., Masters, C. L., Beyreuthers, K. (1992) Substitutions of hydrophobic amino acids reduce the amyloidogenicity of Alzheimer's disease βA4 peptides, *J. Mol. Biol. 228*, 460−473.
34. Fraser, P. E., McLachlan, D. R., Surewicz, W. K., Mizzen, C. A., Snow, A. D., Nguyen, J. T., Kirschner, D. A. (1994) Conformation and fibrillogenesis of Alzheimer Aβ peptides with selected substitution of charged residues, *J. Mol. Biol. 244*, 64−73.
35. Boland, K., Manias, K. Perlmutter, D. H. (1995) Specificity in recognition of amyloid-β peptide by the serpin-enzyme complex receptor in hepatoma cells and neuronal cells, *J. Biol. Chem. 270*, 28022 28028.
36. Soto, C., Castaño, E. M., Frangione, B., Inestrosa, N. C. (1995) The α-helical to β-strand transition in the amino-terminal fragment of the amyloid β-peptide modulates amyloid formation, *J. Biol. Chem. 270*, 3063−3067.
37. Esler, W. P., Stimson, E. R., Ghilardi, J. R., Lu Y. A., Felix, A. M., Vinters, H. V., Mantyh, P. W., Lee, J. P., Maggio, J. E. (1996) Point substitution in the central hydrophobic cluster of a human β-amyloid congener disrupts peptide, *Biochemistry 35*, 13914−13921.
38. Wood, S. J., Wetzel, R., Martin, J. D., Hurle, M. R. (1995) Prolines and amyloidogenicity in fragments of the Alzheimer's peptide β/A4, *Biochemistry 34*, 724 728.
39. Maggio, J. E. and Mantyh, P. W. (1996) Brain amyloid−a physicochemical perspective, *Brain Path. 6*, 147−162.
40. Findeis, M. A., Musso, G. M., Arico-Muendel, C. C., Benjamin, H. W., Hundal, A. M., Lee, J., Chin, J., Kelley, M., Wakefield, J., Hayward, N. J., and Molineaux, S. M. (1999) Modified-peptide inhibitors of amyloid β-peptide polymerization, *Biochemistry 38*, 6791−6800.
41. Soto, C., Sigurdsson, E. M., Morelli, L., Kumar, R. A., Castano, E. M., and Frangione, B. (1998) β-sheet breaker peptides inhibit fibrillogenesis in a rat brain model of amyloidosis: Implications for Alzheimer's therapy, *Nat. Med. 4*, 822−826.
42. Garzon-Rodriguez, W., Vega, A., Sepulveda-Becerra, M., Milton, S., Johnson, D. A., Yatsimirsky, A. K., and Glabe, C. G. (2000) A conformation change in the carboxyl terminus of Alzheimer's Abeta (1−40) accompanies the transition from dimer to fibril as revealed by fluorescence quenching analysis, *J. Biol. Chem. 275*, 22645−22649.
43. Pramanik, B. N., Bartner, P. L., Mirza, U. A., Liu, Y. H., and Ganguly, A. K. (1998) Electrospray ionization mass spectrometry for the study of noncovalent complexes: an emerging technology, *J. Mass. Spectrom. 33*, 911−920.

44. Baca, M., and Kent, S. B. H. (1992) Direct observation of a ternary complex between the dimeric enzyme HIV-1 protease and a substrate-based inhibitor, *J. Am. Chem. Soc. 114*, 3992−3993.
45. Hsieh, Y. L., Cai, J. Y., Li, Y. T., Henion, J. D., and Ganem, B. (1995) Detection of noncovalent FKBP FK506 and FKBP rapamycin complexes by capillary electrophoresis mass-spectrometry and capillary electrophoresis tandem mass-spectrometry, *J. Am. Soc. Mass. Spec. 6*, 85−90.
46. Li, Y. T., Hsieh, Y. L., Henion, J. D., Senko, M. W., McLafferty, F. W., and Ganem, B. (1993) Mass-spectrometric studies on noncovalent dimers of leucine-zipper peptides. *J. Am. Chem. Soc*, *115*, 8409−8413.
47. Egnaczyk, G. F., Greis, K. D., Stimson, E. R., and Maggio, J. E. (2001) Photoaffinity cross-linking of Alzheimer's disease amyloid fibrils reveals interstrand contact regions between assembled beta-amyloid peptide subunits, *Biochemistry 40*, 11706−11714.
48. Dorman, G., and Prestwich, G. D. (1994) Benzophenone photophores in biochemistry. *Biochemistry 33*, 5661−5673.
49. Prestwich, G. D., Dorman, G., Elliott, J. T., Marecak, D. M., and Chaudhary, A. (1997) Benzophenone photoprobes for phosphoinositides, peptides and drugs, *Photochem. Photobiol. 65*, 222−234.
50. LeVine, H. (1995) Thioflavine-T Interactions with Amyloid β-Sheet Structures, *Amyloid—Int. J. Exp. Clin. Invest. 2*, 1−6.
51. Balbach, J. J., Ishii, Y., Antzutkin, O. N., Leapman, R, D., Rizzo, N. W. Dyda, F., Reed, J. and Tycko, R. (2000) Amyloid fibril formation by Aβ16−22, a seven-residue fragment of the alzheimer's β-amyloid peptide, and structural characterization by solid state NMR, *Biochemistry 39*, 13748−13759.
52. Cole, J. L., and Hansen, J. C. (1999) Analytical ultracentrifugation as a contemporary biomolecular research tool, *J. Biomol. Tech. 10*, 163−176.
53. Soreghan, B., Kosmoski, J., and Glabe, C. (1994) Surfactant properties of Alzheimer's Aβ peptides and the mechanism of amyloid aggregation, *J. Biol. Chem. 269*, 28551−28554.
54. Ramakrishnan, C., and Mitra, J. (1978) Dimensions of the ester unit, *Proc. Indian Acad. Sci., Sect. A 87*, 13-21.
55. Arnett, E. M., Mitchell, E. J., and Murty, T. S. S. R. (1974) Comparison of hydrogen-bonding and proton-transfer to some Lewis-bases, *J. Am. Chem. Soc. 96*, 3875−3891.
56. Chen, X. G., Brining, S. K., Nguyen, V. Q., and Yergey, A. L. (1997) Simultaneous assessment of conformation and aggregation of β-amyloid peptide using electrospray ionization mass spectrometry, *FASEB J. 11*, 817−823.
57. Phillips, S. T., Rezac, M., Abel, U., Kossenjans, M., and Bartlett, P. A. (2002) "@-Tides": The 1,2-dihydro-3(6H)-pyridinone unit as a β-strand mimic. *J. Am. Chem. Soc. 124*, 58−66.
58. Harper, J. D., and Lansbury, P. T., Jr. (1997) Models of amyloid seeding in Alzheimer's disease and scrapie: mechanistic truths and physiological consequences of the time-dependent solubility of amyloid proteins, *Annu. Rev. Biochem. 66*, 385−407.
59. Yong, W., Lomakin, A., Kirkitadze, M. D., Teplow, D. B., Chen, S. H., and Benedek, G. B. (2002) Structure determination of micelle-like intermediates in amyloid β-protein fibril assembly by using small angle neutron scattering, *Proc. Natl. Acad. Sci. U.S.A. 99*, 150−154.
60. Lomakin, A., Chung, D. S., Benedek, G. B., Kirschner, D. A., and Teplow, D. B. (1996) On the nucleation and growth of amyloid β-protein fibrils: detection of nuclei and quantitation of rate constants, *Proc. Natl. Acad. Sci. U.S.A. 93*, 1125−1129.
61. Lomakin, A., Teplow, D. B., Kirschner, D. A., and Benedek, G. B. (1997) Kinetic theory of fibrillogenesis of amyloid β-protein, *Proc. Natl. Acad. Sci. U.S.A. 94*, 7942−7947.
62. Bitan, G., Lomakin, A., and Teplow, D. B. (2001) Amyloid β-protein oligomerization: prenucleation interactions revealed by photoinduced cross-linking of unmodified proteins, *J. Biol. Chem. 276*, 35176−35184.

BI0259857